Tensor-Based Near-Field MIMO Channel Estimation and User Localization

Liana Khamidullina, Selibis Sorker, and Martin Haardt
Communication Research Laboratory, Ilmenau University of Technology, Ilmenau, Germany
email:{liana.khamidullina, selibis.sorker, martin.haardt}@tu-ilmenau.de

***Abstract*—As sixth-generation (6G) networks are expected to employ very large antenna arrays, the radiative near-field region correspondingly expands, leading to the breakdown of conventional far-field approximations in many communication scenarios. In this paper, we propose a localization scheme that exploits the spherical wavefront characteristics of electromagnetic fields to achieve high-resolution user positioning and channel parameter estimation. We consider a multi-carrier wireless communication system with a massive two-dimensional antenna array at the base station and employ tensor-based signal processing as well as optimization techniques to localize a multi-antenna user and identify the associated reflected paths in three-dimensional space. We demonstrate that, in the presence of at least three non-line-of-sight (non-LoS) paths, the user can be localized even when the LoS path is blocked or shadowed. Moreover, with appropriate transmit signal design, the proposed algorithm enables semi-blind estimation of the channel parameters and is, therefore, very attractive for integrated sensing and communication applications.**

***Index Terms*—near-field, tensor decomposition, user localization, MIMO channel estimation.**

I. Introduction

In pursuit of achieving peak data rates and high spectral efficiency, 6G networks are envisioned to operate in higher frequency bands and employ increasingly large antenna arrays. Fifth-generation (5G) massive MIMO technology, typically comprising around 64 antenna elements [1], is expected to evolve toward gigantic [2] and extremely large-scale MIMO [1] in 6G. This evolution significantly expands the radiative near-field region, leading to the invalidity of conventional far-field assumptions, such as planar electromagnetic wavefronts and identical phase responses across antenna elements, in many practical scenarios.

Consequently, channel models for large-scale MIMO networks rely on spherical wavefront assumptions, under which both the distances and angles between the source and receiver antennas vary across the array. Although spherical wavefront modeling increases the system complexity and the computational burden, it also offers notable advantages, including more accurate estimation of both distance and angular parameters as well as the ability to perform near-field beamforming or finite-depth beam focusing [1], [2]. This technique enables energy to be focused at different distances along the same direction. Effective beam focusing, however, requires accurate knowledge of the underlying communication channels, which has recently renewed the interest in near-field parameter and channel estimation schemes. Several near-field-based algorithms employ the Fresnel approximation [3], [4], which approximates a spherical wavefront using a second-order Taylor expansion of the true phase distribution of the wavefront across the antenna array. Improved estimation accuracy can be achieved by adopting the exact spherical wavefront model which avoids systematic errors introduced by the Fresnel approximation [5]. Near-field models have also received significant attention in MIMO radar [6]–[8], where spherical wavefronts are exploited for high-resolution positioning. Near-field communication channel estimation and user localization based on uniform linear arrays (ULAs) have been investigated in [9]–[15], while uniform planar arrays (UPAs) and cross arrays are considered in [5], [16], [17].

In this paper, we propose a MIMO extension of the Tensor-Based Near-Field Localization (TeNFiLoc) scheme in [5] for joint channel estimation and user localization. The proposed TeNFiLoc-MIMO algorithm exploits the exact spherical wavefront model to obtain high-resolution estimates of the user's position and velocity, as well as the parameters of the dominant reflected paths. We consider a multi-carrier wireless communication system with a massive antenna array at the base station and employ the canonical polyadic tensor decomposition (CPD) [18] to localize the user and the associated reflected paths. In contrast to the schemes in [5] and [16], we consider a multiple-antenna user and additionally estimate the directions of departure. We also propose a subspace-enhancement approach that exploits both the received pilots and the data symbols to improve the localization accuracy compared to the pilot-based approach in [5]. Moreover, unlike ULA-based approaches, the proposed method enables three-dimensional user localization. We also show that, in the presence of at least three non-line-of-sight (non-LoS) paths, the user can be localized even when the line-of-sight (LoS) path is blocked or shadowed. Finally, with an appropriate signal design, the proposed algorithm enables semi-blind estimation of the channel parameters and is therefore particularly attractive for integrated sensing and communication applications.

II. System Model

We consider an uplink multi-carrier wireless communication system in which a moving user transmits to a base station equipped with a large uniform planar array (UPA) comprising M_{R} antennas. The user is equipped with a planar antenna

The authors gratefully acknowledge the support of the German Research Foundation (DFG) under Grant 402834619 (AdAMMM II, HA 2239/14-3).

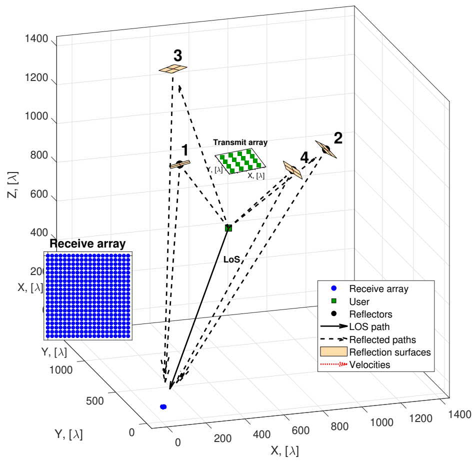

Fig. 1: Scenario geometry with zoomed views of the antenna arrays.

array consisting of M_{T} elements. The Cartesian coordinates of the receive and transmit antennas are denoted by the position vectors $\boldsymbol{p}_{m_{\mathrm{R}}} = [x_{m_{\mathrm{R}}}, y_{m_{\mathrm{R}}}, z_{m_{\mathrm{R}}}]^{\mathrm{T}}$, $m_{\mathrm{R}} \in \{0,\ldots,M_{\mathrm{R}}-1\}$ and $\boldsymbol{p}_{m_{\mathrm{T}}} = [x_{m_{\mathrm{T}}}, y_{m_{\mathrm{T}}}, z_{m_{\mathrm{T}}}]^{\mathrm{T}}$, $m_{\mathrm{T}} \in \{0,\ldots,M_{\mathrm{T}}-1\}$, respectively. While the receive antenna positions are assumed to be known, the transmit antenna positions are unknown. We assume that the signal transmitted by the user propagates to the receiver via L paths, including a possible LoS path. An example scenario is depicted in Fig. 1. The reference receive antenna is located at the origin of the coordinate system.

The ℓ-th channel path is characterized by unknown parameters $\{\alpha_\ell, \rho_\ell^{(\mathrm{X})}, \phi_\ell^{(\mathrm{X})}, \theta_\ell^{(\mathrm{X})}, d_\ell, v_\ell\}$, where (X) corresponds either to (T) (parameter defined w.r.t. the transmitter) or (R) (defined w.r.t. the receiver). The value α_ℓ represents the ℓ-th path's complex gain that depicts such effects as attenuation and random phase shifts due to propagation, absorption, and reflection; $\rho_\ell^{(\mathrm{X})}$, $\phi_\ell^{(\mathrm{X})}$, and $\theta_\ell^{(\mathrm{X})}$ are the distance, azimuth, and elevation, respectively, towards the last reflection along the ℓ-th path (in case of the LoS, it is a user); d_ℓ is the full path distance traveled by the signal along the ℓ-th path (for the LoS path, $d_\ell = \rho_\ell^{(\mathrm{X})}$), and v_ℓ is the relative velocity along the ℓ-th path. The 3D Cartesian coordinates of the reflectors are denoted by $\boldsymbol{r}_\ell$. Our goal is to estimate the parameters of interest for each path including the location of the user described by either the spherical $\boldsymbol{u}_s = [\rho_s, \phi_s, \theta_s]^{\mathrm{T}}$ or the Cartesian $\boldsymbol{u} = [x_s, y_s, z_s]^{\mathrm{T}}$ coordinates of the user's reference antenna.

We consider a system that uses N_f subcarriers, evenly spaced in frequency with a uniform spacing of Δ_f Hertz. The user's location is determined over a frame of N_t consecutive symbols, uniformly sampled every T_0 seconds. Then, assuming narrowband signals on each subcarrier and perfect synchronization, we can express the received uniformly sampled discrete-time baseband signal at the m_{R}-th receive antenna, on the n-th subcarrier in the t-th symbol $y_{m_{\mathrm{R}},n}[t]$ as

$$y_{m_{\mathrm{R}},n}[t] = \sum_{\ell=0}^{L-1} \sum_{m_{\mathrm{T}}=0}^{M_{\mathrm{T}}-1} \alpha_\ell \cdot e^{j2\pi \frac{f_c}{c}\delta^{(\mathrm{R})}_{\ell,m_{\mathrm{R}}}} \cdot e^{j2\pi \frac{f_c}{c}\delta^{(\mathrm{T})}_{\ell,m_{\mathrm{T}}}} \cdot e^{-j2\pi n \Delta_f \tau_\ell} \cdot e^{j2\pi t \frac{f_c T_0}{c} v_\ell} \cdot s_{m_{\mathrm{T}},n}[t] + z_{m_{\mathrm{R}},n}[t], \tag{1}$$

where the ℓ-th path delay from the user's reference antenna to the reference antenna at the receive array is denoted as $\tau_\ell = d_\ell/c$, and c is the speed of light. The Doppler shift of the ℓ-th path is expressed as $f_\ell^d = f_c \cdot v_\ell/c$, where $f_c = f_0 + \Delta_f \cdot N_f/2$ is the carrier (center) frequency. The term $\delta_{\ell,m_{\mathrm{R}}}$, ($\delta_{\ell,m_{\mathrm{T}}}$) denotes the m_{R}-th (m_{T}-th) antenna "geometric" path difference for the ℓ-th path. It is the difference in the distances the wavefront has to travel to the m-th antenna and to the reference antenna. The expression for the path differences using the exact spherical wavefront model at the receive array is given in (2) on the top of the next page. The expression for the transmit array is similar. We always choose $m_{\mathrm{R}}, m_{\mathrm{T}} = 0$ as the reference antenna, which means that $\delta_{\ell,0} = 0$, $\forall \ell$. The complex transmitted signal is denoted as $s_{m_{\mathrm{T}},n}[t]$, and $z_{m_{\mathrm{R}},n}[t]$ is a realization of an independently and identically distributed zero-mean circularly symmetric complex Gaussian noise process with variance σ^2.

For a more compact representation of the received data in (1), we collect the path gains, the space, frequency, and the time exponential terms in the corresponding steering vectors[1] $\boldsymbol{b}_\ell^{(\mathrm{T})} = [1, e^{j2\pi\frac{f_c}{c}\delta^{(\mathrm{T})}_{\ell,1}}, \ldots, e^{j2\pi\frac{f_c}{c}\delta^{(\mathrm{T})}_{\ell,M_{\mathrm{T}}-1}}]^{\mathrm{T}} \in \mathbb{C}^{M_{\mathrm{T}}}$, $\boldsymbol{b}_\ell^{(\mathrm{R})} = [1, e^{j2\pi\frac{f_c}{c}\delta^{(\mathrm{R})}_{\ell,1}}, \ldots, e^{j2\pi\frac{f_c}{c}\delta^{(\mathrm{R})}_{\ell,M_{\mathrm{R}}-1}}]^{\mathrm{T}} \in \mathbb{C}^{M_{\mathrm{R}}}$, $\boldsymbol{b}_\ell^f = [1, e^{-j2\pi\Delta_f\tau_\ell}, \ldots, e^{-j2\pi(N_f-1)\Delta_f\tau_\ell}]^{\mathrm{T}} \in \mathbb{C}^{N_f}$, and $\boldsymbol{b}_\ell^t = [1, e^{j2\pi\frac{f_cT_0}{c}v_\ell}, \ldots, e^{j2\pi(N_t-1)\frac{f_cT_0}{c}v_\ell}]^{\mathrm{T}} \in \mathbb{C}^{N_t}$. By concatenating the steering vectors of L paths, we can construct the transmit, receive, frequency, and time steering matrices $\boldsymbol{B}^{(\mathrm{T})} \in \mathbb{C}^{M_{\mathrm{T}}\times L}$, $\boldsymbol{B}^{(\mathrm{R})} \in \mathbb{C}^{M_{\mathrm{R}}\times L}$, $\boldsymbol{B}^f \in \mathbb{C}^{N_f\times L}$, and $\boldsymbol{B}^t \in \mathbb{C}^{N_t\times L}$, respectively. The vector $\boldsymbol{\alpha} = [\alpha_0, \ldots, \alpha_{L-1}]^{\mathrm{T}} \in \mathbb{C}^L$ collects the complex path gains, and the tensor $\boldsymbol{\mathcal{S}} \in \mathbb{C}^{M_{\mathrm{T}}\times N_f\times N_t}$ contains the transmitted data.

Then, using Matlab array indexing notation, we can represent the received data in (1) in tensor form as

$$[\boldsymbol{\mathcal{Y}}]_{(:,n,t)} = [\boldsymbol{\mathcal{H}}]_{(:,:,n,t)} \cdot [\boldsymbol{\mathcal{S}}]_{(:,n,t)} + [\boldsymbol{\mathcal{Z}}]_{(:,n,t)}, \tag{3}$$

where $\boldsymbol{\mathcal{Z}}$ collects noise terms $z_{m_{\mathrm{R}},n}[t]$. The tensor $\boldsymbol{\mathcal{H}} \in \mathbb{C}^{M_{\mathrm{R}}\times M_{\mathrm{T}}\times N_f\times N_t}$ represents the communication channel which can be expressed using the space, time, and frequency steering matrices in the form of a CPD as

$$\boldsymbol{\mathcal{H}} = \boldsymbol{\mathcal{D}}_4\left\{\boldsymbol{\alpha}\right\} \times_1 \boldsymbol{B}^{(\mathrm{R})} \times_2 \boldsymbol{B}^{(\mathrm{T})} \times_3 \boldsymbol{B}^f \times_4 \boldsymbol{B}^t. \tag{4}$$

Assuming that within each coherence block, M_{T} pilot sequences are transmitted sequentially, one from each transmit antenna, the initial channel estimate can be obtained from the stacked pilot observations

$$\tilde{\boldsymbol{\mathcal{H}}} = \boldsymbol{\mathcal{D}}_4\left\{\boldsymbol{\alpha}\right\} \times_1 \boldsymbol{B}^{(\mathrm{R})} \times_2 \boldsymbol{B}^{(\mathrm{T})} \times_3 \boldsymbol{B}^f \times_4 \boldsymbol{B}^t + \tilde{\boldsymbol{\mathcal{Z}}}. \tag{5}$$

The low rank tensor decomposition can also be applied under the assumption of unknown transmitted data if the transmitted data follows a rank-1 tensor structure such that

[1] *Notation.* Matrices and vectors are denoted by upper-case ($\boldsymbol{A}$) and lower-case ($\boldsymbol{a}$) bold-faced letters, respectively. Bold-faced calligraphic letters denote tensors ($\boldsymbol{\mathcal{A}}$). The superscript $\{\cdot\}^{\mathrm{T}}$ denotes the matrix transpose. We use $\circ$ and $\times_n$ to denote the outer and the n-mode products [18], respectively. The operators $\boldsymbol{D}\left\{\boldsymbol{a}\right\}$ and $\boldsymbol{\mathcal{D}}_R\left\{\boldsymbol{a}\right\}$ denote the operation of constructing a diagonal matrix and the diagonal tensor [18] from the vector $\boldsymbol{a}$. For matrices, $\overline{\boldsymbol{A}}$ and $\underline{\boldsymbol{A}}$ denote the matrix $\boldsymbol{A}$ with its last row and first row removed, respectively.

$$\delta^{(\mathrm{R})}_{\ell,m_{\mathrm{R}}} = \|\boldsymbol{p}_{m_{\mathrm{R}}} - \boldsymbol{r}_\ell\| - \|\boldsymbol{p}_0 - \boldsymbol{r}_\ell\| = \sqrt{(x_{m_{\mathrm{R}}} - x_\ell)^2 + (y_{m_{\mathrm{R}}} - y_\ell)^2 + (z_{m_{\mathrm{R}}} - z_\ell)^2} - \rho^{(\mathrm{R})}_\ell \quad \forall m \tag{2}$$

$\boldsymbol{\mathcal{S}} = \boldsymbol{s}''' \circ \boldsymbol{s}' \circ \boldsymbol{s}''^{\mathrm{T}}$, where $\boldsymbol{s}' = [s'_0, s'_1, \ldots, s'_{N_f-1}]^{\mathrm{T}} \in \mathbb{C}^{N_f}$, $\boldsymbol{s}'' = [s''_0, s''_1, \ldots, s'_{N_t-1}]^{\mathrm{T}} \in \mathbb{C}^{N_t}$, and $\boldsymbol{s}''' = [s'''_0, s'''_1, \ldots, s'_{M_{\mathrm{T}}-1}]^{\mathrm{T}} \in \mathbb{C}^{M_{\mathrm{T}}}$. Then, the received data tensor $\boldsymbol{\mathcal{Y}} \in \mathbb{C}^{M_{\mathrm{R}} \times N_f \times N_t}$ can be expressed as

$$\boldsymbol{\mathcal{D}}_3\left\{\boldsymbol{\gamma}\right\} \times_1 \boldsymbol{B}^{(\mathrm{R})} \times_2 \left(\boldsymbol{D}\left\{\boldsymbol{s}'\right\}\boldsymbol{B}^f\right) \times_3 \left(\boldsymbol{D}\left\{\boldsymbol{s}''\right\}\boldsymbol{B}^t\right) + \boldsymbol{\mathcal{Z}}, \tag{6}$$

which is also a noise-corrupted low-rank CPD.

III. Tensor-Based Near-Field MIMO Localization algorithm (TeNFiLoc-MIMO)

The proposed channel parameters and user localization algorithm consist of five main steps, as described below.

A. Estimation of the steering matrices

The first step of the algorithm is to estimate the steering matrices $\boldsymbol{B}^{(\mathrm{R})}$, $\boldsymbol{B}^{(\mathrm{T})}$, $\boldsymbol{B}^f$, and $\boldsymbol{B}^t$, which can be performed via an approximate low-rank CPD of the received data tensor $\boldsymbol{\mathcal{Y}}$ under the unknown data assumption[2] or the CPD of the tensor $\tilde{\boldsymbol{\mathcal{H}}}$ in the known data case (OFDM training phase).

In our simulations, among other methods, we employ the SECSI framework [19] to compute the CPD. SECSI is a subspace-based method that first computes a truncated Tucker decomposition [18] of the tensor and subsequently recovers the CPD factors from the estimated multilinear subspaces.

From (6), it can be seen that $\boldsymbol{B}^{(\mathrm{R})}$ is independent of the transmitted data. Therefore, instead of estimating the receive spatial subspace from $\tilde{\boldsymbol{\mathcal{H}}}$, we estimate it from the full received data tensor $\boldsymbol{\mathcal{Y}}$, whose mode-1 unfolding contains significantly more observations. The improved subspace estimate replaces the corresponding Tucker factor of $\tilde{\boldsymbol{\mathcal{H}}}$, and can be used to recompute the core and the channel tensors. The updated truncated Tucker decomposition is then passed to SECSI for CPD factor extraction, yielding a more accurate estimate of $\boldsymbol{B}^{(\mathrm{R})}$. Although demonstrated here using SECSI, the same principle can be applied to other subspace-based CPD algorithms[3].

The path gains can be computed using the first elements of the estimated factor matrices as

$$\hat{\alpha}_\ell = [\hat{\boldsymbol{B}}^{(\mathrm{R})}]_{(0,\ell)} \cdot [\hat{\boldsymbol{B}}^{(\mathrm{T})}]_{(0,\ell)} \cdot [\hat{\boldsymbol{B}}^{f}]_{(0,\ell)} \cdot [\hat{\boldsymbol{B}}^{t}]_{(0,\ell)}, \forall \ell. \tag{7}$$

The scaling ambiguity inherent in the CPD can be corrected by dividing the columns of the estimated steering matrices by their first element, since the steering matrices are assumed to have ones in the first row.

B. Estimation of path distances and relative velocities

In the next step, we estimate the path distances $\hat{d}_\ell$ and the relative velocities $\hat{v}_\ell$ using the shift invariance property of the Vandermonde matrices in the time and the frequency domain as[4] $\hat{\boldsymbol{d}} = -\frac{c}{2\pi\Delta_f}\angle\left(\boldsymbol{D}\left\{(\overline{\boldsymbol{B}}^f)^H\underline{\boldsymbol{B}}^f\right\}\right) \in \mathbb{R}^L$ and $\hat{\boldsymbol{v}} = \frac{c}{2\pi f_c T_0}\angle\left(\boldsymbol{D}\left\{(\overline{\boldsymbol{B}}^t)^H\underline{\boldsymbol{B}}^t\right\}\right) \in \mathbb{R}^L$.

C. Localization of the last reflection points

For each path, the last reflection point is described via the $\rho^{(\mathrm{R})}_\ell$, $\phi^{(\mathrm{R})}_\ell$, and $\theta^{(\mathrm{R})}_\ell$ parameters which can be estimated from $\boldsymbol{B}^{(\mathrm{R})}$ using a localization approach described in [5], where the location coordinates are computed using the path differences $\delta^{(\mathrm{R})}_{\ell,m_{\mathrm{R}}}$ estimated after the initial phase unwrapping procedure expressed as $\hat{\boldsymbol{\delta}}^{(\mathrm{R})}_\ell = \frac{\lambda}{2\pi} \cdot \mathcal{U}\{\angle\hat{\boldsymbol{b}}^{(\mathrm{R})}_\ell\}$, where $\hat{\boldsymbol{\delta}}^{(\mathrm{R})}_\ell \in \mathbb{C}^{M_{\mathrm{R}}}$ is the vector of path difference estimates and $\mathcal{U}\{\cdot\}$ denotes the unwrapping algorithm [20], [21]. Next, using (2), the estimated path differences and the known receive antenna coordinates (for planar arrays, $z_{m_{\mathrm{R}}} = 0$), we can construct a system of linear equations

$$2\begin{bmatrix} x_1 & y_1 & \hat{\delta}_{\ell,1} \\ \vdots & \vdots & \vdots \\ x_{M_{\mathrm{R}}-1} & y_{M_{\mathrm{R}}-1} & \hat{\delta}_{\ell,M_{\mathrm{R}}-1} \end{bmatrix} \boldsymbol{p}_\ell = \begin{bmatrix} d_1^2 - \hat{\delta}^2_{\ell,1} \\ \vdots \\ d^2_{M_{\mathrm{R}}-1} - \hat{\delta}^2_{\ell,M_{\mathrm{R}}-1} \end{bmatrix}, \tag{8}$$

which can be solved for the location vector $\boldsymbol{p}_\ell = [x_\ell, y_\ell, \sqrt{x_\ell^2 + y_\ell^2 + z_\ell^2}]^{\mathrm{T}}$ using the least squares solution. Then, the spherical coordinates of the reflection points can be calculated as $\rho_\ell = (\hat{\boldsymbol{p}}_\ell)_{(3)}$, $\phi_\ell = \operatorname{atan2}\left(\frac{[\hat{\boldsymbol{p}}_\ell]_{(2)}}{\rho_\ell}, \frac{[\hat{\boldsymbol{p}}_\ell]_{(1)}}{\rho_\ell}\right)$, and $\theta_\ell = \cos^{-1}\left(\frac{\sqrt{[\hat{\boldsymbol{p}}_\ell]^2_{(1)} + [\hat{\boldsymbol{p}}_\ell]^2_{(2)}}}{\rho_\ell}\right)$ (valid in half of the 3D space).

D. User localization

For the user localization step, we consider two scenarios: LoS and non-LoS. In the first case, $\rho_\ell = d_\ell$, therefore, the index of the most suitable candidate path for the LoS path can be determined by $\ell_{\mathrm{LoS}} = \arg\min_\ell |\hat{d}_\ell - \hat{\rho}_\ell|$ and the condition $1 - \delta \leq \frac{\hat{d}_{\ell_{\mathrm{LoS}}}}{\hat{\rho}_{\ell_{\mathrm{LoS}}}} \leq 1 + \delta$, where $0 < \delta \leq 1$ is some arbitrary threshold. If the condition is satisfied, the user location is determined as $\hat{\boldsymbol{u}} = \hat{\boldsymbol{r}}_{\ell_{\mathrm{LoS}}}$.

In a scenario where a LoS is not present among the obtained path estimates, we can still construct a system of linear equations based on the fact that the distance between the reflectors and the user is equal to the difference between the full path distance d_ℓ and the $\rho^{(\mathrm{R})}_\ell$ which has been estimated in the previous steps. Thus, to estimate the user's location (reference point), we minimize the least squares cost function

$$f(\boldsymbol{u}) = \sum_{\ell=0}^{L-1} w_\ell \Big(\|\boldsymbol{u} - \hat{\boldsymbol{r}}_\ell\| - \hat{d}_\ell + \hat{\rho}^{(\mathrm{R})}_\ell\Big)^2 \tag{9}$$

where $\hat{\boldsymbol{r}}_\ell$ denotes the estimated location of the ℓ-th reflector in Cartesian coordinates, $\big[\boldsymbol{w}\big]_{(\ell)} = w_\ell = |\hat{\alpha}_\ell|^2/\|\hat{\boldsymbol{\alpha}}\|^2$ is the ℓ-th path weighting coefficient, and $\boldsymbol{\alpha} \in \mathbb{C}^L$ is the vector

[2] Although in the semi-blind case we do not estimate the transmit steering vectors, the parameter estimation and the user localization can still be performed using the receive steering vectors.

[3] An alternative approach is to compute the coupled CPD of $\tilde{\boldsymbol{\mathcal{H}}}$ and $\boldsymbol{\mathcal{Y}}$, which, however, entails a higher computational complexity compared to the updated subspace approach described above.

[4] In case of the unknown data assumption (semi-blind case), the approximate CPD provides the "modulated" estimates of the time and frequency steering matrices $\boldsymbol{D}\left\{\boldsymbol{s}'\right\}\boldsymbol{B}^f$, and $\boldsymbol{D}\left\{\boldsymbol{s}''\right\}\boldsymbol{B}^t$. To "demodulate" the matrices and estimate $\boldsymbol{s}$ and $\boldsymbol{\mu}$, Algorithm 1 of [5] can be employed.

of all path gains. The system in (9) has a unique solution if the number of non-LoS paths is not less than three (since we estimate three unknowns: x_s, y_s, and z_s).

E. Estimation of the transmit array parameters

The estimation of the transmit side parameters requires the knowledge of the parameters (orientation) of the antenna panel, which can be determined using the estimated transmit side path differences $\hat{\boldsymbol{\delta}}_\ell^{(\mathrm{T})} = \frac{\lambda}{2\pi} \cdot \mathcal{U}\{\angle \hat{\boldsymbol{b}}_\ell^{(\mathrm{T})}\}, \forall \ell$, the user location $\hat{\boldsymbol{u}}$, and the locations of the reflectors $\hat{\boldsymbol{r}}_\ell$. To determine the antenna position (other than the reference antenna), we employ the definition of the path differences in (2) (for the transmitter side) and construct the cost function

$$f(\boldsymbol{p}_{m_\mathrm{T}}) = \sum_{\ell=0}^{L-1} w_\ell \Big(\|\boldsymbol{p}_{m_\mathrm{T}} - \hat{\boldsymbol{r}}_\ell\| - \|\hat{\boldsymbol{u}} - \hat{\boldsymbol{r}}_\ell\| - \hat{\delta}_{\ell,m_\mathrm{T}}^{(\mathrm{T})} \Big)^2, \quad (10)$$

where $\boldsymbol{p}_{m_\mathrm{T}}$ is the m_Tth antenna position ($m_\mathrm{T} = \{1, \ldots, M_\mathrm{T} - 1\}$). Minimizing (10) for $\boldsymbol{p}_{m_\mathrm{T}}$ allows determining the transmit antenna array orientation, and, consequently, the DoDs.

IV. Simulation Results

For the simulations, we consider an OFDM system with $f_c = 60$ GHz, yielding a wavelength of $\lambda = c/f_c \approx 5$ mm. The system has pilot tones evenly distributed across frequency and time, filling the full bandwidth and frame duration. We assume that the total number of subcarriers is $N_f^d = 2048$, the effective pilot subcarrier spacing is $\Delta_f = 5.76$ MHz, and the total number of pilot subcarriers is $N_f = 85$. The parameter estimation procedure is assumed to be carried out over a frame of $N_t^d = 1120$ OFDM symbols, and only each $k_t = 42$-nd of them contains pilot tones, which results in a total number of $N_t = 26$ pilot symbols. The receiving and the transmitting arrays are uniform rectangular arrays (URAs) of size 20×20 and 4×4, respectively. The simulation scenario is also illustrated in Fig. 1. The user is located at $\boldsymbol{u} = [2.5, 2.5, 3.536]$ [m] and moves away from the receive array with a velocity of $v_0 = 1$ m/s. Moreover, we assume that there are $L_\mathrm{r} = 4$ reflected paths with reflector coordinates $x_\ell = \{1.25, 5, 1.875, 3.75\}$, $y_\ell = \{2.5, 2.5, 5, 1.25\}$, and $z_\ell = \{5.303, 5.303, 6.894, 5.303\}$ [m]. We assume that each reflected path is additionally attenuated by 3 dB relative to the LoS path. The performance is evaluated using the root mean squared error (RMSE) of the Euclidean distance between the true ($\boldsymbol{u}$) and the estimated ($\hat{\boldsymbol{u}}_{\boldsymbol{k}}$) location of the user (reflector) [5] or via the normalized mean squared error (NMSE) of the reconstructed channel tensor. We average the results over 1000 simulation trials.

The simulation results are depicted in Fig. 2. The dashed line represents half of the minimum separation distance between the paths. For Figs. 2(a), 2(b), and 2(c), we change the SNR and show the user localization accuracy (LoS and non-LoS scenarios) and the channel reconstruction error. We compare the following algorithms: "TeNFiLoc-MIMO (SECSI)" refers to the proposed algorithm using the SECSI framework with "CON-PS" heuristic for computing the CPD [19]; "TeNFiLoc-MIMO (Closed-Form)" denotes the use of the closed-form CPD algorithm from [22]; and "TeNFiLoc-MIMO (Tensorlab NLS)" refers to use of the NLS CPD algorithm from [23]. As can be observed, the "TeNFiLoc-MIMO (SECSI)" approach outperforms the NLS and closed-form algorithms, as SECSI shows better accuracy in highly correlated factor-matrix scenarios [19]. In Fig. 2(a), we additionally compare the user localization performance with the 3D Unitary Tensor ESPRIT (UTE) algorithm [24], which uses the far-field assumption, and therefore shows an inferior performance. The "Pilots", "Blind", and "Full-Data" in the legend of Figs. 2(a) and 2(b) refer to the estimation approach described in Section III-A. As it can be seen, the proposed subspace combining approach noticeably improves the localization accuracy. Moreover, given the distance to the user in the simulation setup, Figs. 2(a) and 2(b) show that the user localization is possible beyond the Fresnel region when the LoS path is present or the SNR is high enough. It should be noted that the overall time complexity of the TeNFiLoc-MIMO scheme is dominated by the complexity of the CPD. Depending on the complexity-accuracy requirements, the appropriate CPD can be selected. While the SECSI approach provides better accuracy, the closed-form solution is less complex.

Fig. 2(d) shows the localization accuracy of the user and the reflectors ("R-ℓ", where R-1 is the closest to the receiver) in a non-LoS case as the distance between the reflectors and the user changes, revealing a degradation in accuracy as the user and the reflectors move towards the far-field region. "MIXED, $\delta = 30\%$" refers to the approach described in Section III-D, (δ is the LoS path threshold) which uses (9) if the LoS path condition is not satisfied. The "NLS" denotes that the user is always localized by minimizing (9). The "MIXED" approach has the same performance as the "NLS" approach, since it correctly determines whether the scenario has a LoS path. The user localization accuracy is lower than that of the reflectors and degrades faster because (9) uses distance estimates for all paths to form the cost function, and these estimates degrade as the distance to the receiver increases.

V. Conclusions

In this paper, we propose TeNFiLoc-MIMO, a MIMO extension of the TeNFiLoc framework for joint channel estimation and user localization. Using the CPD and the exact spherical wavefront model, the proposed method estimates the user position, velocity, directions of departure, and the parameters of the dominant reflected paths. Furthermore, we propose a subspace-enhancement approach that exploits both pilots and data symbols to improve the estimation accuracy. The simulation results demonstrate that the TeNFiLoc-MIMO framework accurately estimates the channel and localization parameters in both LoS and non-LoS scenarios. The proposed subspace-enhancement approach provides a noticeable improvement over pilot-only processing. Moreover, the results confirm that user localization remains possible even in the absence of a LoS path, provided that at least three non-LoS paths are available. These features make TeNFiLoc-MIMO a promising solution for future integrated sensing and communication systems.

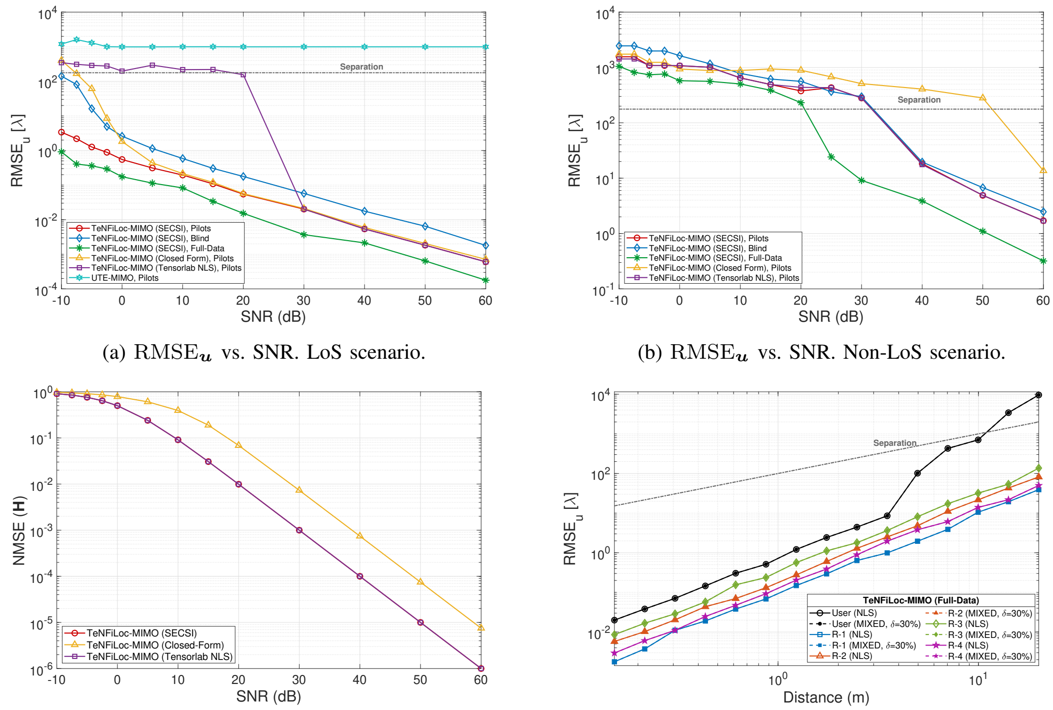

(a) $\mathrm{RMSE}_{\boldsymbol{u}}$ vs. SNR. LoS scenario.

(b) $\mathrm{RMSE}_{\boldsymbol{u}}$ vs. SNR. Non-LoS scenario.

(c) NMSE of the reconstructed $\boldsymbol{\mathcal{H}}$ vs. SNR. Non-LoS scenario.

(d) $\mathrm{RMSE}_{\boldsymbol{u}}$ vs. Distance. Non-LoS scenario. $\mathrm{SNR} = 30$ dB.

Fig. 2: Localization and channel estimation accuracy.

References

[1] H. Lei, J. Zhang, Z. Wang, B. Ai, and E. Björnson, "Near-Field User Localization and Channel Estimation for XL-MIMO Systems: Fundamentals, Recent Advances, and Outlooks," *IEEE Wireless Communications*, vol. 32, no. 4, pp. 190–198, 2025.

[2] E. Björnson, F. Kara, N. Kolomvakis, A. Kosasih, P. Ramezani, and M. B. Salman, "Enabling 6G Performance in the Upper Mid-Band by Transitioning From Massive to Gigantic MIMO," *IEEE Open Journal of the Communications Society*, vol. 6, pp. 5450–5463, 2025.

[3] A. M. Elbir, W. Shi, A. K. Papazafeiropoulos, P. Kourtessis, and S. Chatzinotas, "Near-Field Terahertz Communications: Model-Based and Model-Free Channel Estimation," *IEEE Access*, vol. 11, 2023.

[4] H. Li, Z. Wang, X. Mu, P. Zhiwen, and Y. Liu, "Near-Field Integrated Sensing, Positioning, and Communication: A Downlink and Uplink Framework," *IEEE Journal on Selected Areas in Communications*, vol. 42, no. 9, pp. 2196–2212, 2024.

[5] I. Podkurkov, G. Seidl, L. Khamidullina, A. Nadeev, and M. Haardt, "Tensor-Based Near-Field Localization Using Massive Antenna Arrays," *IEEE Transactions on Signal Processing*, vol. 69, pp. 5830–5845, 2021.

[6] L. Khamidullina, I. Podkurkov, and M. Haardt, "Conditional and Unconditional Cramér-Rao Bounds for Near-Field Localization in Bistatic MIMO Radar Systems," *IEEE Transactions on Signal Processing*, vol. 69, pp. 3220–3234, May 2021.

[7] H. Wang, Z. Xiao, and Y. Zeng, "Cramér-Rao Bounds for Near-Field Sensing With Extremely Large-Scale MIMO," *IEEE Transactions on Signal Processing*, vol. 72, pp. 701–717, 2024.

[8] N. Xie, S. Ouyang, K. Liao, H. Wang, and J. Jiang, "Near-Field Multiple Target Localization in Frequency Diverse Array Based on Tensor Decomposition," *Remote Sensing*, vol. 14, no. 17, 2022.

[9] S. Liu, X. Yu, Z. Gao, J. Xu, D. W. K. Ng, and S. Cui, "Sensing-Enhanced Channel Estimation for Near-Field XL-MIMO Systems," *IEEE Journal on Selected Areas in Communications*, vol. 43, no. 3, pp. 628–643, 2025.

[10] Y. Zhu, H. Guo, and V. K. N. Lau, "Bayesian Channel Estimation in Multi-User Massive MIMO With Extremely Large Antenna Array," *IEEE Transactions on Signal Processing*, vol. 69, pp. 5463–5478, 2021.

[11] Y. Chen and L. Dai, "Non-Stationary Channel Estimation for Extremely Large-Scale MIMO," *IEEE Transactions on Wireless Communications*, vol. 23, no. 7, pp. 7683–7697, 2024.

[12] X. Wu, J. Qiu, J. Sun, W. Liu, H. Zhang, and Y. Eldar, "Source Localization for Extremely Large-Scale Antenna Arrays under Spatial Non-Stationarity and Near-Field Effects," *IEEE Transactions on Signal Processing*, vol. PP, pp. 1–16, 01 2026.

[13] S. Cheng, L. You, Z. Jin, L. Cheng, and X. Gao, "Tensor-Based Channel Estimation for Near-Field Millimeter Wave XL-MIMO Systems," *IEEE Wireless Communications Letters*, vol. 14, no. 7, pp. 1909–1913, 2025.

[14] A. Shahmansoori, G. E. Garcia, G. Destino, G. Seco-Granados, and H. Wymeersch, "Position and Orientation Estimation Through Millimeter-Wave MIMO in 5G Systems," *IEEE Transactions on Wireless Communications*, vol. 17, no. 3, pp. 1822–1835, 2018.

[15] Y. Lu and L. Dai, "Near-field channel estimation in mixed los/nlos environments for extremely large-scale mimo systems," *IEEE Transactions on Communications*, vol. 71, no. 6, pp. 3694–3707, 2023.

[16] Z. Lu, Y. Han, S. Jin, and M. Matthaiou, "Near-Field Localization and Channel Reconstruction for ELAA Systems," *IEEE Transactions on Wireless Communications*, vol. 23, no. 7, pp. 6938–6953, 2024.

[17] Z. Jiang, H. Chen, W. Liu, and G. Wang, "3-D temporal-spatial-based near-field source localization considering amplitude attenuation," *Signal Processing*, vol. 201, p. 108735, 2022.

[18] T. G. Kolda and B. W. Bader, "Tensor Decompositions and Applications," *SIAM Review*, vol. 51, no. 3, pp. 455–500, 2009.

[19] F. Roemer and M. Haardt, "A semi-algebraic framework for approximate CP decompositions via Simultaneous Matrix Diagonalizations (SECSI)," *Elsevier Signal Processing*, vol. 93, no. 9, pp. 2722–2738, Sep. 2013.

[20] K. Itoh, "Analysis of the phase unwrapping problem," *Applied Optics*, vol. 21, no. 14, p. 2470, Jul. 1982.

[21] D. C. Ghiglia and M. D. Pritt, *Two-Dimensional Phase Unwrapping: Theory, Algorithms, and Software*. Wiley New York, 1998, vol. 4.

[22] Y. Lin, S. Jin, M. Matthaiou, and X. You, "Structured Tensor Decomposition-Based Channel Estimation for Wideband Millimeter Wave MIMO," in *Proc. 53rd Asilomar Conference on Signals, Systems, and Computers*, Pacific Grove, CA, USA, Nov. 2019, pp. 421–426.

[23] N. Vervliet, O. Debals, L. Sorber, M. van Barel, and L. De Lathauwer, "Tensorlab 3.0," Mar. 2016. [Online]. Available: https://www.tensorlab.net/

[24] M. Haardt, F. Roemer, and G. Del Galdo, "Higher-Order SVD-Based Subspace Estimation to Improve the Parameter Estimation Accuracy in Multi-dimensional Harmonic Retrieval Problems," *IEEE Transactions on Signal Processing*, vol. 56, pp. 3198–3213, Jul. 2008.